INTERNATIONAL VIDEO JOURNAL OF ENGINEERING RESEARCH, Vol. 1, 71–82 (1991)

NUMERICAL SIMULATIONS OF DOUBLE-DIFFUSIVE CONVECTION IN A HELE–SHAW CELL

C. BECKERMANN*, C. FAN† AND J. MIHAILOVIC‡
Department of Mechanical Engineering, University of Iowa, Iowa City, IA 52242, U.S.A.

SUMMARY

A study is reported of double-diffusive convection in a Hele–Shaw cell. The system consists of two horizontal fluid layers of different concentration destabilized by lateral heating/cooling. The governing transport equations are solved using the flux-corrected transport algorithm, which is known to possess the numerical properties of stability, accuracy, monotonicity, and conservation. Good agreement with simultaneous experiments is obtained. Numerical simulations are performed for a wide range of stability numbers, N. The video of the results reveals a number of highly unsteady double-diffusive convection phenomena associated with the interaction, breakdown, merging, and mixing of the fluid layers.

NOMENCLATURE

c	specific heat (J kg K^{-1})
C	concentration (kg kg^{-1})
d	gap width (m)
D	mass diffusivity (m^2 s^{-1})
g	gravitational acceleration (m s^{-2})
K	permeability (m^2)
L	length or height of enclosure (m)
Le	Lewis number, see equation (5b)
N	stability number, see equation (5c)
Nu	Nusselt number, see equation (8)
Ra	Rayleigh number, see equation (5a)
s	wall thickness (m)
t	dimensionless time, $t'u_0\rho_f c_f/[L(\rho c)_e]$
T	temperature (K)
u	dimensionless x-direction velocity, u'/u_0
u_0	reference velocity, Ra α_e/L ($m^{-1}s$)
v	dimensionless y-direction velocity, v'/u_0
W	total width of Hele–Shaw cell (m)
x	dimensionless horizontal coordinate, x'/L
y	dimensionless vertical coordinate, y'/L

Greek symbols

α_e	effective thermal diffusivity (m^2/s)
β_C	coefficient of solutal expansion

* Assistant Professor
† Visiting Scholar
‡ Research Assistant

1052–9268/91/020071–12$06.00

Received 15 March 1991
Revised 8 October 1991

β_T coefficient of thermal expansion (K^{-1})
θ dimensionless temperature, $(T - T_2)/(T_1 - T_2)$
μ dynamic viscosity (Ns m^{-2})
ρ density (kg m^{-3}
σ thermal capacitance ratio, see equation (5d)
ϕ dimensionless concentration, $(C - C_1)/(C_2 - C_1)$
ψ dimensionless stream function, $\psi'/(Lu_0)$

Subscripts
e effective
f fluid
m mixing
w wall
1 left wall
2 right wall

Superscripts
' dimensional value

1. INTRODUCTION

Double-diffusive natural convection involving the simultaneous interaction of heat and solute occurs in many industrial and natural processes and displays a range of complex flow structures.[1] Recently, the formation of convecting layers has been observed in various crystal growth systems[2,3] and during solidification of binary solutions.[4] These layers are solutally well-mixed and separated by thin interfaces resulting in a steplike density distribution in the vertical direction. Recirculating fluid motion within each layer is driven through side wall heating/cooling. Owing to solute transport across the interfaces, the solute concentration differences between the layers decrease with time, the interfaces eventually become unstable and the layers break down and merge.[5]

Several investigations have considered solutally stratified solutions, with a linear gradient, destabilized by lateral heating (see, for example, Reference 6). The stability limits for incipient layer formation have been established and the subsequent layer interaction and merging have been studied (see Reference 7 and the references therein). Double-diffusive layer interaction and merging has also been studied for a somewhat more simple system consisting of two discrete layers of different concentration heated or cooled from the vertical walls of an enclosure.[8-11] These studies investigate both experimentally and numerically the transient system behavior, including the lateral heat transfer and the interfacial species transfer.

The present study considers a similar system as that studied by Wirtz[9] and Bergman and Ungan;[11] however, the enclosure is a Hele–Shaw cell. A Hele–Shaw cell consists of a narrow slot sandwiched between parallel walls. There exists a direct mathematical similarity between two-dimensional flow in a porous medium and laminar flow in a Hele–Shaw cell.[12] For low Reynolds numbers both flows are governed by Darcy's law. Owing to the absence of macroscopic inertia and viscous terms, Darcy's law is much simpler than the full Navier–Stokes equations. Although convection phenomena in porous media are generally different from those in pure fluids, Griffiths[13] found that the entire range of double-diffusive fluid motions encountered in pure fluids (i.e. fingers and layers) is displayed. Since its walls can be made transparent, the Hele–Shaw cell lends itself especially well as a laboratory apparatus to study two-dimensional convection patterns. Because of the small thickness of the

fluid layer between the walls, distortion of flow visualization images by the strong refractive index gradients present in double-diffusive systems is minimized.

This study represents high-resolution numerical simulations of double-diffusive natural convection in a Hele–Shaw cell together with some experimental validation. Generally, double-diffusive convection is transient and characterized by very sharp species concentration gradients at non-stationary interfaces separating fluids of different concentration. This represents a formidable challenge for most numerical techniques. Wirtz[9] utilized centered difference operators to obtain stable and accurate predictions for a layered double-diffusive system. However, this technique is limited to relatively small Rayleigh numbers and it is questionable whether all double-diffusive flow phenomena were adequately resolved with the 17×17 grid used by Wirtz.[9] Heinrich[14] used a finite element algorithm based on the penalty function and Petrov–Galerkin concepts in simulating double-diffusive convection in an initially linearly stratified system and obtained good agreement with experiments. Beckermann and Viskanta[4] employed the control-volume formulation together with the power-law scheme[15] in their numerical simulation of double-diffusive convection in a solidifying binary solution. While the flow structures were qualitatively predicted correctly, the results were subject to considerable numerical diffusion. In the present work, the flux-corrected transport (FCT) finite difference method[16] is applied to the simulation of double-diffusive convection. As noted by Gross *et al.*,[17] the FCT method possesses four desirable numerical properties: stability, accuracy, monotonicity and conservation,[16,18–20] and greatly reduces numerical diffusion.

2. GOVERNING EQUATIONS

The physical system considered is shown in Figure 1. The cell is square with walls of length and height L. The width of the cell is W and the gap size is d. The horizontal top and bottom walls are adiabatic, while the vertical sidewalls are isothermal. Initially, two hydrodynamically stable fluid layers of equal height ($L/2$) and temperature (T_2) but different solute concentration (C_1 and C_2) are contained within the cell. At time $t = 0$, the left sidewall temperature is

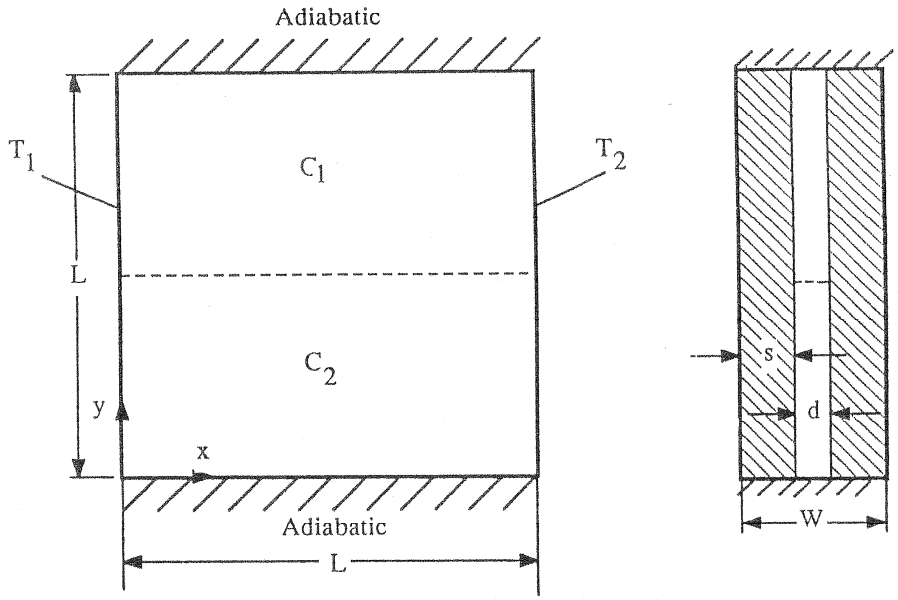

Figure 1. Schematic of the physical system

suddenly raised to T_1. We assume that thermal equilibrium exists between the walls and the fluid, Darcy's law is applicable, the solution is dilute, the density is a linear function of temperature and solute concentration, and the Boussinesq approximation applies whereby all thermophysical properties are constant except the density in the buoyancy term in the momentum equation.

The governing equations can be written in dimensionless form as

$$\frac{\partial^2\psi}{\partial x^2}+\frac{\partial^2\psi}{\partial y^2}=-\frac{\partial\theta}{\partial x}+N\frac{\partial\sigma}{\partial x} \tag{1}$$

$$\frac{\partial\theta}{\partial t}+\frac{\partial}{\partial x}(u\theta)+\frac{\partial}{\partial y}(v\theta)=\frac{1}{\mathrm{Ra}}\left(\frac{\partial^2\theta}{\partial x^2}+\frac{\partial^2\theta}{\partial y^2}\right) \tag{2}$$

$$\frac{\partial\phi}{\partial t}+\frac{\partial}{\partial x}(\sigma u\phi)+\frac{\partial}{\partial y}(\sigma v\phi)=\frac{1}{\mathrm{RaLe}}\left(\frac{\partial^2\phi}{\partial x^2}+\frac{\partial^2\phi}{\partial y^2}\right) \tag{3}$$

where

$$u=\frac{\partial\psi}{\partial y} \tag{4a}$$

$$v=-\frac{\partial\psi}{\partial x} \tag{4b}$$

All symbols are defined in the Nomenclature. Since the flow in the layers is thermally driven, the velocity scale (Ra α_e/L) is appropriate. The governing dimensionless parameters appearing in the above equations are

$$\mathrm{Ra}=\frac{\rho_f g\beta_T(T_1-T_2)KL}{\mu\alpha_e} \quad \text{Rayleigh number} \tag{5a}$$

$$\mathrm{Le}=\alpha_e/D \quad \text{Lewis number} \tag{5b}$$

$$N=\frac{\beta_C(C_2-C_1)}{\beta_T(T_1-T_2)} \quad \text{stability number} \tag{5c}$$

$$\sigma=\frac{(\rho c)_e W}{d\rho_f c_f} \quad \text{thermal capacitance ratio} \tag{5d}$$

Note that the Raleigh number contains the permeability and that the effective thermal diffusivity, α_e, is given by $k_e/(\rho c)_e$, where k_e is the effective thermal conductivity and $(\rho c)_e$ is the effective thermal capacitance. For a Hele–Shaw cell, the permeability and effective properties can be calculated from:[12]

$$K=\frac{d^3}{12W} \tag{6a}$$

$$k_e=k_f d/W+k_w(1-d/W) \tag{6b}$$

$$(\rho c)_e=\rho_f c_f d/W+\rho_w c_w(1-d/W) \tag{6c}$$

The initial and boundary conditions are

$$\theta = 0, \quad \phi = \begin{cases} 1 & 0 \leqslant y < 0{\cdot}5 \\ 0 & 0{\cdot}5 \leqslant y \leqslant 1 \end{cases}, \quad \psi = 0 \qquad \text{for } t = 0 \tag{7a}$$

$$\frac{\partial \theta}{\partial y} = \frac{\partial \phi}{\partial y} = 0, \quad \psi = 0 \qquad \text{for } y = 0,1 \tag{7b}$$

$$\theta = 1, \quad \frac{\partial \phi}{\partial x} = 0, \quad \psi = 0 \qquad \text{for } x = 0 \tag{7c}$$

$$\theta = 0, \quad \frac{\partial \phi}{\partial x} = 0, \quad \psi = 0 \qquad \text{for } x = 1 \tag{7d}$$

The average Nusselt numbers at the left and right side walls are given by

$$\mathrm{Nu}_{0,1} = \int_0^1 \left. \frac{\partial \theta}{\partial x} \right|_{x=0,1} \mathrm{d}y \tag{8}$$

3. NUMERICAL PROCEDURES

The transport equations (2) and (3) were solved numerically using the two-dimensional FCT scheme. All details of this method have been described by Book,[16] Gross and Baer,[18] Book and Fry,[21] Barr and Ashurst,[20] and Baer and Gross[19] and do not need to be repeated here. In brief, antidiffusive fluxes are computed that reduce diffusive errors to sixth order. A two time step approach is used in this explicit method in order to maintain second order time accuracy. The stream function equation (1) is solved using the stabilized error vector propagation (EVP) method described by Roache[22] which is a direct method for the solution of Poisson type equations. A detailed description of the computer implementations can be found in the work of Baer and Gross.[19] The application of FCT to high Rayleigh number convection in a porous medium is summarized by Gross *et al.*,[17] together with some validation of the method.

Considerable effort was spent to ensure time step and grid size independence in the present application. All results reported in this paper are obtained using a Courant number of 0·2 and a 101×101 uniform grid. Figure 2 shows a typical comparison of concentration profiles obtained using different grid sizes. This figure also demonstrates the ability of the FCT method to resolve steep concentration gradients accurately. Results using a finer grid are virtually indistinguishable from those using the 101×101 grid. The same is true for smaller time steps. The Nusselt numbers at steady state agree to within 0·2% with the results of Shiralkar *et al.*[23] for thermal natural convection in a vertical porous cavity (see also below). It should be noted that preliminary calculations for $\mathrm{Ra} > 1000$ (not reported here) appear to require a finer grid than that used here.

The computations were performed on an IBM 3090-200E/VF supercomputer. The FCT method lends itself to considerable vectorization and much of the computer time is spent using the direct EVP solver. Each numerical simulation requires many thousand time steps to reach steady state. A dimensionless time interval of unity represents about 500 numerical time steps and requires approximately 600 sec of CPU time. The video was generated using the public-domain NCSA Image software on a Macintosh II computer.

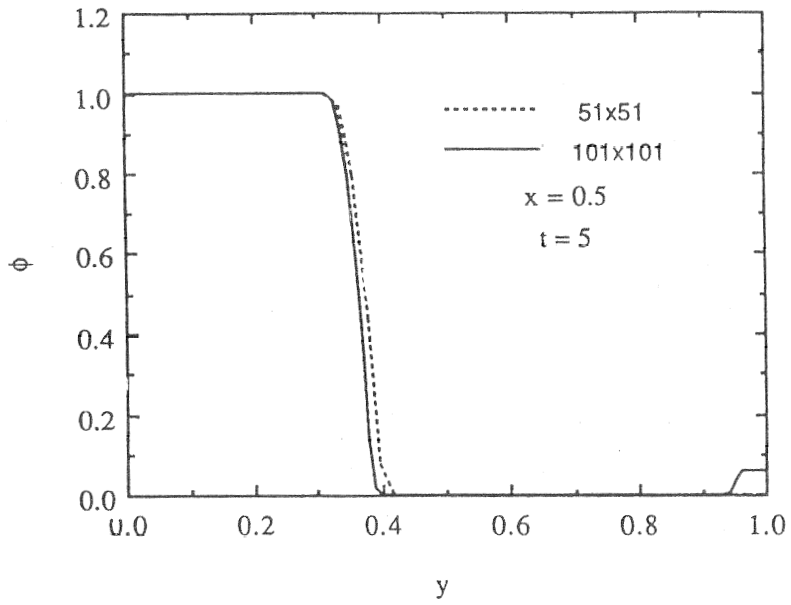

Figure 2. Comparison of concentration profiles obtained using different grids

4. EXPERIMENTAL TECHNIQUES

Experiments were formed in a Hele–Shaw cell having dimensions $L = 51{\cdot}3$ mm, $d = 1{\cdot}6$ mm, and $s = 6{\cdot}5$ mm. The front and back walls consisted of pyrex glass plates. The glass plates were held in place by thin spacers attached to the vertical sidewalls outside of the test section. These spacers blocked some of the view of the test section, making the photographs of the experiment (see Plate I) slightly non-square. The vertical sidewalls were made of multipass copper heat exchangers, through which temperature-regulated water was circulated. Thermocouples embedded near the surface of the heat exchangers indicated that the sidewalls were isothermal to within $\pm 0{\cdot}1^{\circ}$ C of the desired hot and cold wall temperatures. The top and bottom walls consisted of low thermal conductivity phenolic sheet. Except when photographs were taken, the whole apparatus was encased in 5 cm thick foam insulation. To reduce the thermal interaction with the environment further, the mean cell temperature was exactly maintained at room temperature.

The two layer system was established by carefully introducing pure water ($C_1 = 0$) above a layer of $KMnO_4$ solution of concentration C_2. The aqueous $KMnO_4$ solution was chosen because it is clearly visible at very low concentrations. The interface between the two layers (at $y = 1/2$) was observed to be very sharp at the onset of the experiments. Prior to the start of an experiment the test cell was held at a uniform temperature T_2 by circulating water from one constant temperature bath through both heat exchangers, while another bath was preheated to T_1. At the onset of an experiment, valves were switched to increase the temperature impulsively of one of the heat exchangers to T_1. Owing to the thermal inertia of the heat exchanger, it took about 30 sec for it to reach the desired temperature (for a total experiment duration of more than three hours).

5. RESULTS AND DISCUSSION

Comparison of numerical and experimental results

Although a number of experiments were performed, the results of only one experiment are reported here for the purpose of validating the numerical data. In this experiment, the

temperature difference ($T_1 - T_2$) was 5° C, while the concentration difference ($C_2 - C_1$) was 0·165 wt% $KMnO_4$. The values of the governing dimensionless parameters are: Ra = 50·8, Le = 438·5, $N = 1{\cdot}0$, and $\sigma = 4{\cdot}11$. There is an uncertainty of about 5% in the values of these parameters, because of uncertainties in the values of the thermophysical properties, the temperatures, and the initial concentration difference. It should be noted that the experiment was repeated several times and the time associated with the mixing of the layers (see below) was repeatable to within better than 5%.

Plate I shows representative photographs of the experiment (left panel) together with color plots of numerically predicted concentration fields (right panel). Although quantitative concentration measurements were not performed, the photographs clearly show the transient evolution of the double-diffusive layers in the experiment. The location and shape of the double-diffusive interface between the two layers are very sensitive to the system parameters and the heat and mass transfer phenomena within the layers, and serve well as a tool for validation. It can be seen that there is excellent agreement between the experimental and numerical results before layer turnover and mixing (Plates I(a) and I(b)). The predicted layer turnover time is equal to 290 min ($t_m = 200$), while the experimental value is only 3 min higher. Plate I(e) shows the results shortly after the onset of mixing ($t = 202$). Here, considerable differences can be observed between the measured and predicted flow structures. This can be attributed to the highly transient and chaotic nature of the mixing process. By repeating the experiment several times, it was observed that slight differences in the onset of the interface instabilities cause large variations in the flow structure at later times. In other words, the 3 min difference in the layer turnover time makes comparison between the experimental and numerical results difficult during the ensuing mixing process. However, the general system behavior appeared to be always similar. Although the mixing process deserves further research attention, the above comparisons established some confidence in the numerical results. A detailed discussion of the various physical phenomena occurring in the present system is provided in the following section.

Video

The video shows numerical simulations of three test cases corresponding to $N = 0{\cdot}5$, $1{\cdot}0$, and $1{\cdot}5$ and Ra = 500, Le = 100 and $\sigma = 1{\cdot}0$. A thermal capacitance ratio of unity would be difficult to achieve in an experiment; however, this value is chosen for simplicity. A Lewis number of 100 is characteristic of many salt–water systems, and a Rayleigh number of 500 can be considered intermediate. The Nusselt number for steady thermal natural convection in a porous cavity (or Hele–Shaw cell) heated/cooled from the sides is approximately equal to 8·95 for Ra = 500.[23] This study focuses on the basic heat and mass transfer phenomena for various stability numbers. For each case, the video shows the transient evolution of the concentration field, which is followed by the temperature and streamfunction fields. Each color represents a certain value of the field variable, with the color palette and the dimensionless time t provided below the cell. Experiments are not shown on the video because of their long duration.

For $N = 0{\cdot}5$, the layers are very unstable. At the left wall, heated fluid rises up and lifts the initially horizontal interface between the layers of different concentration. Because of the large value of the Lewis number, the fluid retains its composition, while the temperature non-uniformities propagate relatively quickly through the cell. Owing to solute transport across the interface, the top layer fluid flowing along the interface attains a higher concentration. However, no fluid appears directly to penetrate the interface between the layers of different concentration and the interface retains its sharpness and smooth appearance until about $t = 9$.

The interface continues to stretch and deform as it turns and passes along the top wall. With increasing distance from the left, hot wall, the temperature of the high concentration fluid behind the interface gradually decreases. Eventually, this results in an unstable situation, where fluid of a higher density overlies fluid of a lower density (and concentration C_1). Thus, at about $t = 10$ a so-called 'double-diffusive finger'[1] forms through which high concentration fluid flows downward through the fluid of concentration C_1. This time (t_m) marks the beginning of the layer turnover and mixing regime. Note that the finger has a mushroom-shaped tip characteristic of buoyant plumes. Within a very short time several such fingers develop as the thermal boundary layer at the left wall continually supplies high concentration fluid to the top of the cell, at the expense of the bottom layer. Often, the fingers themselves are unstable, break up into two or more plumes, and eventually mix with the fluid in the upper layer. At about $t = 25$, the bottom layer is virtually depleted of high concentration fluid and the entire cell is filled with double-diffusive fingers of various shapes. After about $t = 30$, the streamfunction fields show a single, thermally driven recirculation cell. The remaining concentration non-uniformities are advected in a clockwise fashion and produce some unsteadiness mainly in the core of the recirculation cell (see also below). The simulation was terminated at $t = 65$ when the fluid reaches an almost uniform concentration equal to 0·5. The isotherms and streamlines are now identical with those predicted for the steady, two-dimensional, natural thermal convection of a pure fluid in a porous cavity (or Hele–Shaw cell) at Ra = 500.[23]

The convection phenomena are somewhat different for $N = 1{\cdot}0$ and $1{\cdot}5$. Owing to the higher value of the stability number, the thermal buoyancy forces are not able to cause the rapid layer turnover and mixing observed in the $N = 0{\cdot}5$ case. The interface between the fluid layers remains tilted from the horizontal for a long time. Each layer contains a thermally driven, clockwise rotating recirculation cell. For both $N = 1{\cdot}0$, $1{\cdot}5$, the system reaches a thermally quasi-steady regime at about $t = 60$, at which time the temperature gradients at the hot and cold walls are, on the average, equal (see also below). Again, the rapid diffusion of heat relative to that of solute is characteristic of double-diffusive systems due to the large value

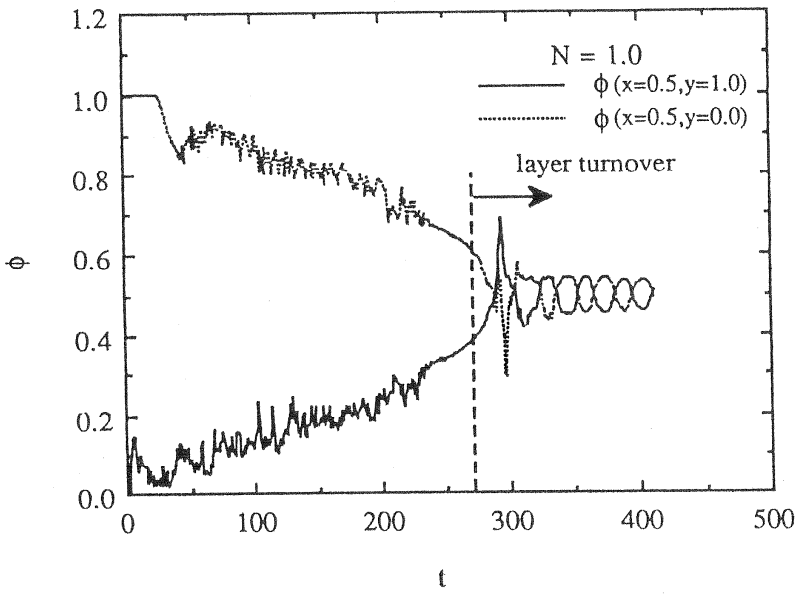

Figure 3. Transient variation of concentrations at two specified points (Ra = 500, $N = 1{\cdot}0$, Le = 100, $\sigma = 1$)

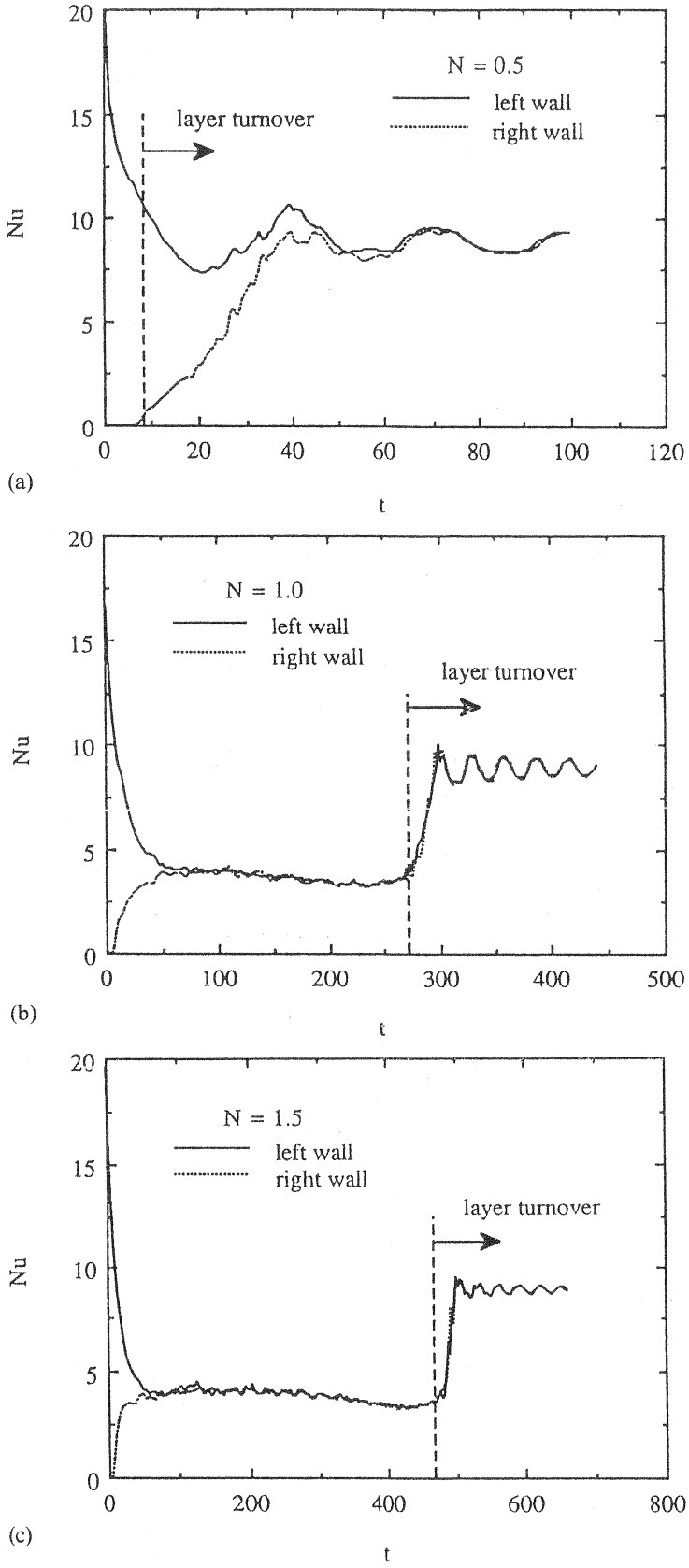

Figure 4. Transient variation of the Nusselt numbers (Ra = 500, Le = 100, $\sigma = 1$)

(a) $N = 0{\cdot}5$;
(b) $N = 1{\cdot}0$;
(c) $N = 1{\cdot}5$.

of the Lewis number. During the thermally quasi-steady regime, the concentration and streamfunction fields are fairly antisymmetric about the cell diagonal. The fluid motion in the layers causes convection of solute across the interface; however, no fluid penetrates the interface at the hot and cold walls. The resulting concentration non-uniformities are advected with the flow in each fluid layer. As fluid of a higher (lower) concentration flows along the top (bottom) wall, its temperature decreases (increases) and a succession of small double-diffusive fingers or plumes develops (while the layers are still stable). This is further illustrated in Figure 3, where the temporal evolution of the concentrations at the points ($x = 0{\cdot}5$, $y = 1{\cdot}0$) and ($x = 0{\cdot}5$, $y = 0{\cdot}0$) is plotted for $N = 1{\cdot}0$. The fluctuations up to about $t = 230$ are due to the plumes passing by these points.

Owing to continued solute transfer across the interface, the concentration difference between the layers and, hence, the stabilizing force of the system decreases and the interface becomes more sloped. At about $t = 230$ for $N = 1{\cdot}0$ and $t = 430$ for $N = 1{\cdot}5$, the interface in the centre region of the cell is almost vertical. Note that the curves in Figure 3 are now more smooth. Eventually, the interface is tilted such that some high concentration fluid overlies low concentration fluid, which is conducive to the formation of double-diffusive fingers. Thust, at $t = 273$ for $N = 1{\cdot}0$ and $t = 470$ for $N = 1{\cdot}5$ the interface at about the cell mid-point becomes unstable and the layer turnover and mixing regime starts. As for $N = 0{\cdot}5$, the mixing process is very vigorous and the streamfunction fields show the merging of the two recirculation cells into a single one. The remaining concentration non-uniformities are advected in a clockwise fashion within the cell. This can also be seen in Figure 3 (for $N = 1{\cdot}0$), where the two concentrations plotted oscillate in a periodic fashion about $0{\cdot}5$. For all N tested, the dimensionless frequency of these oscillations is equal to $3{\cdot}51 \times 10^{-2}$; in other words, it takes $\Delta t = 28{\cdot}5$ for the fluid to make a complete revolution in the cell. Since the flow is thermally driven, this frequency is, of course, different for other Rayleigh numbers. At long times, the oscillations diminish in amplitude because of continued mixing. As for $N = 0{\cdot}5$, the temperature and streamfunction fields are characteristic of thermal natural convection of a pure fluid at approximately $\Delta t = 60$ after the onset of the layer turnover regime (t_m).

The time variation of the Nusselt numbers at the hot and cold walls is shown in Figure 4 for $N = 0{\cdot}5$, $1{\cdot}0$ and $1{\cdot}5$. Initially, the heat flux at the left wall rapidly decreases, while the heat flux at the right wall increases from zero. For all N tested, the system reaches the thermally quasi-steady regime at about $t = 60$, after which the two Nusselt number curves coincide almost exactly. During the quasi-steady regime (except for $N = 0{\cdot}5$), the Nusselt numbers decrease slightly and undergo small fluctuations. This can be attributed to the changing tilt of the double-diffusive interface and the intermittent behavior of the double-diffusive plumes. At the onset of mixing ($t = t_m$), the Nusselt numbers increase sharply and then oscillate about the steady state value with the same period as the concentrations shown in Figure 3. The extrapolated steady state value for Nu is the same for all N and agrees to within $0{\cdot}2\%$ with the numerical result of Shiralkar *et al.*[23] for $\mathrm{Ra} = 500$. The sudden increase in the Nusselt number is due to the two convection cells merging into a single one, which advects the heat more effectively across the cavity. Note that the Nusselt numbers at the hot and cold walls oscillate in phase. The amplitude of the oscillations slowly decreases with time until a constant steady state value is reached.

6. CONCLUSIONS

The video of the present numerical simulations reveals a number of highly unsteady transport phenomena that might have remained undetected without proper visualization (see for example

Reference 9). The layer interaction, merging, and mixing as well as the transient behavior of the lateral heat transfer are investigated in detail for a range of stability numbers. Overall, the general system dynamics in the Hele–Shaw cell are similar to those observed in a cavity of larger width (between the front and back walls).[7,9–11] Obviously, quantitative comparisons are not possible.

The flux-corrected transport algorithm appears to be well suited for the numerical simulation of double-diffusive flows, as witnessed by the good agreement with experiment. However, the chaotic mixing process after layer turnover deserves further research attention. Note that the general form of the present heat and solute transport equations is the same as for applications not involving a Hele–Shaw cell or a porous medium. It should be mentioned that preliminary simulations at much higher Rayleigh numbers show significant small-scale instabilities at the interface between the layers, indicating the need for a much finer grid than that used here. Alternatively, one should develop a sub-grid 'turbulence' model for double-diffusive flows.

Finally, as already mentioned by Beckermann and Viskanta,[4,5] the observed double-diffusive transport phenomena have a profound influence on the chemical and structural homogeneity of a solidifying alloy or crystal. Accurate numerical simulations of the double-diffusive flows in the melt are needed for realistic predictions of potential non-uniformities in the solid.

ACKNOWLEDGEMENTS

The work reported in this paper was supported, in part, by the National Science Foundation under Grant No. CTS-8957149. Computer facilities were made available by the University of Iowa WEEG Computing Center. The authors are indebted to Dr M. R. Baer of Sandia National Laboratories for providing the FCT and EVP solvers.

REFERENCES

1. J. S. Turner, *Buoyancy Effects in Fluids*, Cambridge University Press, Cambridge, 1979.
2. Y. Kamotami, L. W. Wang, S. Ostrach and H. D. Jiang, 'Experimental Study of Natural Convection in Shallow Enclosures with Horizontal Temperature and Concentration Gradients, *Int. J. Heat Mass Transfer,* **28**, 165–173 (1985).
3. L. W. Wang and P. C. Chueng, Flow patterns of natural convection in enclosures with horizontal temperature and concentration gradients, in C. L. Tien *et al.* (eds.), *Proceedings of the 8th International Heat Transfer Conference*, 1986, pp. 1477–1481.
4. C. Beckermann and R. Viskanta, 'Double-diffusive convection during dendritic solidification of a binary mixture', *Physico Chemical Hydrodynamics*, **10**, 195–213 (1988).
5. C. Beckermann and R. Viskanta, 'An experimental study of solidification of binary mixtures with double-diffusive convection in the liquid', *Chemical Engineering Communications*, **85**, 135–156 (1989).
6. S. A. Thorpe, P. K. Hutt and R. Soulsby, 'The effect of horizontal gradients on thermohaline convection', *J. Fluid Mechanics,* **38**, 375–400 (1969).
7. J. Lee, M. T. Hyung and Y. S. Kang, 'Confined natural convection due to lateral heating in a stably stratified solution', *Int. J. Heat Mass Transfer,* **33**, 869–875 (1990).
8. R. A. Wirtz and C. S. Reddy, 'Heat and mass transport across diffusive interfaces bounded by turbulent convecting regions', *Int. J. Heat Mass Transfer*, **19**, 471–478 (1976).
9. R. A. Wirtz, 'The effect of solute layering on lateral heat transfer in an enclosure', *Int. J. Heat Mass Transfer*, **20**, 841–846 (1977).
10. R. A. Wirtz and S. C. Reddy, 'Experiments on convective layer formation and merging in a differentially heated slot', *J. Fluid Mechanics*, **91**, 451–464 (1979).

11. T. L. Bergman and A. Ungan, 'A note on lateral heating in a double diffusive system', *J. Fluid Mechanics*, **194**, 175–186 (1988).
12. B. K. Hartline and C. R. B. Lister, 'Thermal convection in a Hele–Shaw Cell', *J. Fluid Mechanics*, **79**, 379–389 (1977).
13. R. W. Griffiths, 'Layered double-diffusive convection in porous media', *J. Fluid Mechanics*, **102**, 221–248 (1981).
14. J. C. Heinrich, 'A finite element model for double-diffusive flows', *Int. J. Num. Meth. Eng.*, **20**, 447–464 (1984).
15. S. V. Patankar, *Numerical Heat Transfer and Fluid Flow*, McGraw-Hill, New York, 1980.
16. D. L. Book, *Finite-Difference Techniques for Vectorized Fluid Dynamics Calculations*, Springer-Verlag, New York, 1981.
17. R. J. Gross, M. R. Baer and C. E. Hickox, 'The application of flux-corrected transport (FCT) to high Rayleigh number natural convection in porous medium', in C. L. Tien *et al.*, (eds.), *Proceedings of the 8th International Heat Transfer Conference*, pp. 2641–2646, 1986.
18. R. J. Gross and M. R. Baer, 'ETBFCT – a solver for one-dimensional transport equations', Sandia National Laboratories, Report No. 85-1273, 1985.
19. M. R. Baer and R. J. Gross, 'A two-dimensional flux-corrected solver for convectively dominated flows', Sandia National Laboratories, Report No. 85-0613, 1985.
20. P. K. Barr and W. T. Ashurst, 'Evaluation of Zalesak's flux-corrected transport algorithm for convection and diffusion', Sandia National Laboratories, Report No. SAND81-8233, 1982.
21. D. L. Book and M. A. Fry, 'Airblast simulations using flux-corrected transport codes', NRL Report No. 5334, 1984.
22. P. J. Roache, 'Finite difference methods for the steady-state Navier–Stokes equations', Sandia National Laboratories, Report No. SC-RR-72-04 19, 1972.
23. G. S. Shiralkar, M. Haajizadeh and C. L. Tien, 'Numerical study of high Rayleigh number convection in a vertical porous enclosure', *Numerical Heat Transfer*, **6**, 223–234 (1983).

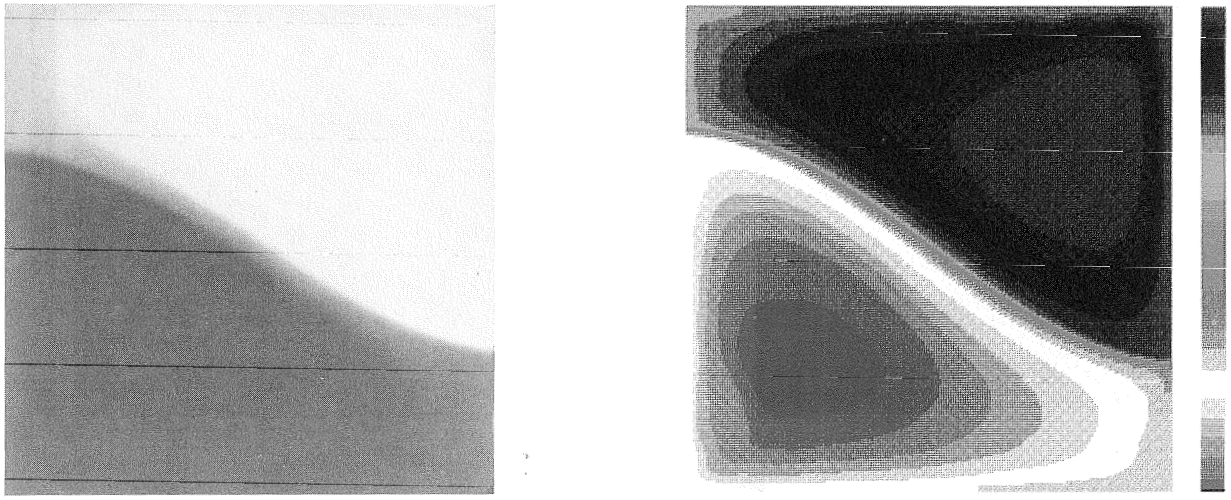

(a)

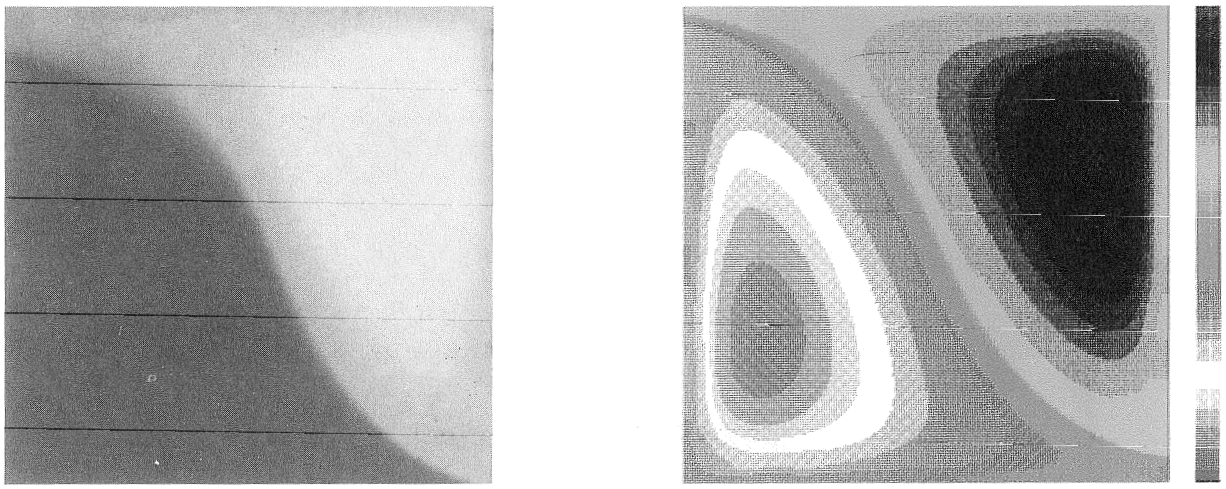

(b)

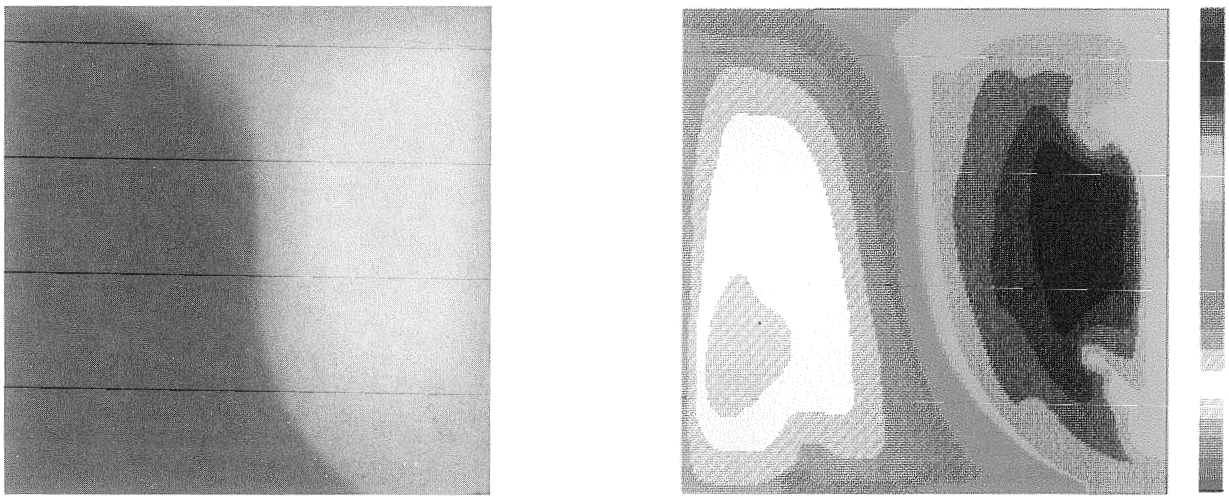

(c)

Plate I (Beckermann *et al.*). Comparison of experimental results (left panel) with predicted concentration fields (right panel) for Ra = 50.8, $N = 1.0$, Le = 438.5 and $\sigma = 4.11$. (a) $t = 50$; (b) $t = 160$; (c) $t = 190$; (d) $t = 199$; (e) $t = 202$

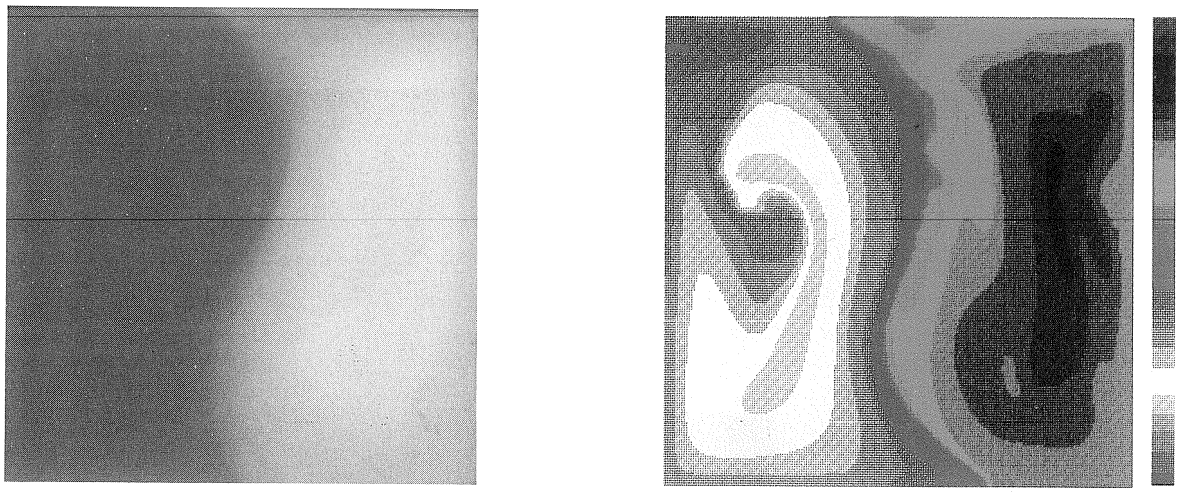

(d)

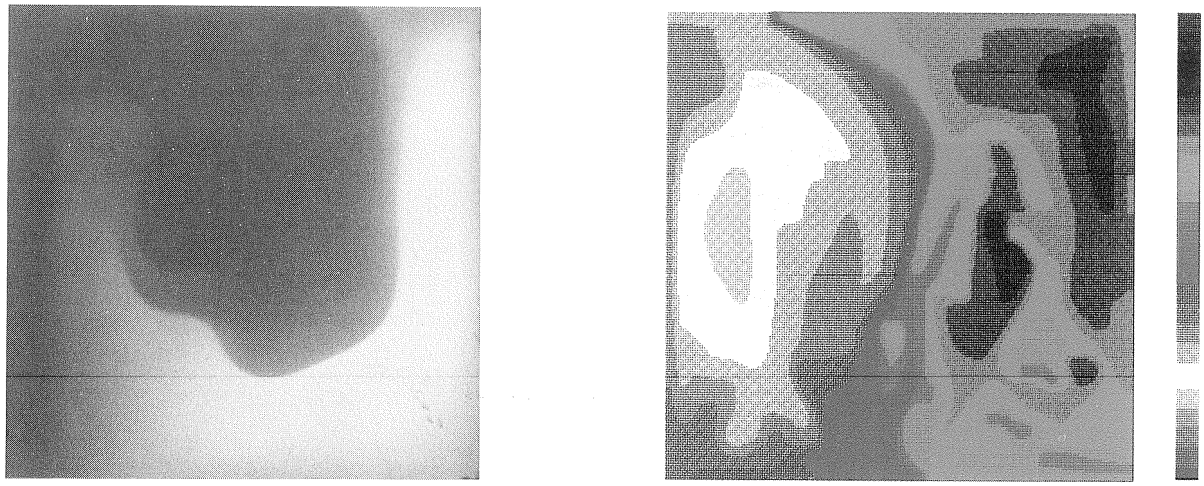

(e)

Plate I (Beckermann *et al.*) continued